

# Population receptive field estimates for motion-defined stimuli

Anna E. Hughes<sup>1,2\*</sup>, John A. Greenwood<sup>1</sup>, Nonie J. Finlayson<sup>1,3</sup> and D. Samuel Schwarzkopf<sup>1,4</sup>

<sup>1</sup> Experimental Psychology, University College London, 26 Bedford Way, London, UK, WC1H 0AP

\* Correspondence: [a.hughes2@exeter.ac.uk](mailto:a.hughes2@exeter.ac.uk); Tel.: +447752549141

## Abstract:

The processing of motion changes throughout the visual hierarchy, from spatially restricted 'local motion' in early visual cortex to more complex large-field 'global motion' at later stages. Here we used functional magnetic resonance imaging (fMRI) to examine spatially selective responses in these areas related to the processing of random-dot stimuli defined by differences in motion. We used population receptive field (pRF) analyses to map retinotopic cortex using bar stimuli comprising coherently moving dots. In the first experiment, we used three separate background conditions: no background dots (dot-defined bar-only), dots moving coherently in the opposite direction to the bar (kinetic boundary) and dots moving incoherently in random directions (global motion). Clear retinotopic maps were obtained for the bar-only and kinetic-boundary conditions across visual areas V1-V3 and also in higher dorsal areas. For the global-motion condition, retinotopic maps were much weaker in early areas only and became clear only in higher areas, consistent with the emergence of global-motion processing in these areas. However, in a second experiment we found very similar results when the bar was low in visibility, with the clearest maps obtained in dorsal extrastriate cortex. This was the case both for a transparent-motion stimulus as well as a bar defined by a static low-level property (dot size) that should have driven responses particularly in V1. In fact, these extrastriate maps only manifested in participants who reported seeing this low-visibility stimulus. Our findings therefore indicate that dorsal extrastriate retinotopic maps may primarily be determined by general stimulus visibility (or salience) and suggests that claims about stimulus selectivity from pRF experiments must be interpreted with caution.

**Keywords:** vision, motion, population receptive field analysis.

## Present addresses:

<sup>2</sup> Centre for Life and Environmental Sciences, University of Exeter, Penryn Campus, Penryn, UK, TR10 9FE

<sup>3</sup> School of Psychology, The University of Queensland, St Lucia QLD 4072, Australia

<sup>4</sup> School of Optometry and Vision Science, University of Auckland, 85 Park Road, Auckland, New Zealand

## 1. Introduction

Motion perception is one of the fundamental dimensions of vision (**Nakayama, 1985; Nishida, 2011**), and it is now known that many areas of the brain are involved in motion processing (**Dupont et al., 1994; Pitzalis et al., 2010; Sunaert et al., 1999; Tootell et al., 1997**). Converging psychophysical, electrophysiological, and imaging evidence suggests that motion is processed in a hierarchical manner, with signals first being processed locally (within restricted spatial windows) in areas such as V1 and then combined at higher levels in the visual cortical hierarchy to generate global motion percepts over larger regions of the visual field (**Adelson and Movshon, 1982; Braddick et al., 2001; Van Essen and Gallant, 1994; Williams and Sekuler, 1984**).

Many psychophysical studies have used tasks involving the detection or discrimination of coherent motion to study the distinction between local- and global-motion processing (**Britten et al., 1993, 1992; Newsome and Paré, 1988; Scase et al., 1996; Watamaniuk, 1993**). Due to the aperture problem, direction-selective neurons in lower visual areas such as V1 are thought to process only local motion – the 1D motion orthogonal to the orientation of the edge that is passing through the receptive field (**Adelson and Movshon, 1982; Marr and Ullman, 1981; Wallach, 1935**). To be able to process global motion, these 1D signals must be integrated over a relatively wide visual field area/region, a process thought to occur in higher visual areas, such as V5/MT+ to generate a global motion direction (**Heeger et al., 1996; Simoncelli and Heeger, 1998**). fMRI evidence has provided support for a distinction in the neural locations of global and local processing, showing that V1 was activated more by incoherent local noise than coherent global motion, perhaps because the noise stimulus led to the activation of neurons with a wider range of motion selectivities. The reverse pattern was seen in V5 and V3A, which both responded more to coherent motion compared to the noise stimulus (**Braddick et al., 2001**).

Other brain regions may be specialized for the detection of more complex motion patterns. One example is that of kinetic boundaries, where an edge is defined by differences in coherent motion direction on either side of the edge. A specific brain region known as the Kinetic Occipital area (KO; also known as V3B) may be specialized for detecting these boundaries (**Van Oostende et al., 1997**). However, other research suggests that KO may also respond preferentially to stimuli such as form cues (**Zeki et al., 2003**), and that because its proposed position overlaps with other visual areas, including LO-1 and LO-2, it is unlikely to be uniquely involved in boundary processing (**Larsson and Heeger, 2006**). Despite this debate over the specificity of the area responding to kinetic contours, it is clear that kinetic boundaries are relatively complex stimuli that are not processed at lower levels in the visual hierarchy: they produce little fMRI response in lower visual areas such as V1 and V2

(**Van Oostende et al., 1997; Zeki et al., 2003**), consistent with electrophysiological evidence that these areas do not have many cells that respond to kinetic contours (**Leventhal et al., 1998; Marcar et al., 2000**).

The visual hierarchy also has multiple representations of the retina, laid out in topological maps that are commonly called retinotopic maps (**Felleman and Van Essen, 1991; Sereno et al., 1995**). While it was once thought that retinotopy was a property of lower level visual areas, it is now known that areas such as MT+ and MST also contain retinotopic maps (TO1 and TO2 respectively) (**Amano et al., 2009**), as do the frontal eye fields (**Kastner et al., 2007**) and even the default mode network (**Knapen et al., 2018**). Indeed, despite the large receptive field sizes within primate MT/V5, it is possible to track object position at the population level (**Chen et al., 2015**). This suggests that retinotopy is a general organizing principle within the cortex. It is therefore of interest to know whether retinotopic map properties vary according to the visual area under question, and particularly whether these properties are affected by the different functional selectivities of different regions of the brain.

One technique that has been used to analyse retinotopic maps via fMRI is population receptive field (pRF) analysis, providing an estimation of the visual field position preferred by each voxel and the range of visual field locations where a stimulus evokes a response (**Dumoulin and Wandell, 2008**). pRFs can therefore be thought of as a statistical summary of the neuronal properties within a sampled region. Recent work has shown systematic differences in pRF sizes across different brain regions and eccentricities, with size increasing along the visual processing hierarchy and with increasing eccentricity (**Alvarez et al., 2015; Amano et al., 2009; Dumoulin and Wandell, 2008; Haas et al., 2014; Harvey and Dumoulin, 2011; Schwarzkopf et al., 2014**).

Across these different brain areas, a number of factors can affect pRF size and position. Retinotopy in early visual areas is primarily thought to be stimulus-driven, but there is evidence that higher level maps can also be attentionally-driven (**Tootell et al., 1998**). One study (**Saygin and Sereno, 2008**) used point light biological walkers moving in a ‘wedge’ stimulus to dissociate attention and stimulus effects in retinotopic mapping, and showed that V1 did not respond clearly when the distinction between stimulus and background was driven only attentionally, but it did respond when there was a visual difference between stimulus and background without attention directed to the stimulus. The opposite pattern was seen in frontal and parietal areas. The spatial tuning of pRFs is also affected by attentional load at fixation, with pRF size increasing and pRF location becoming more eccentric under high perceptual load (**Haas et al., 2014**). Similar results have also been reported in face-selective brain regions (**Kay et al., 2015**). This position modulation seems to occur across the entire visual field, not just at the attended location (**Klein et al., 2014**), and recent work suggests that these

position shifts are the key mechanism by which attention enhances discriminability and representational quality of stimuli (**Vo et al., 2017**). It therefore seems that attention can affect cortical spatial tuning properties, in turn altering the visibility of stimulus differences.

Stimulus properties may also alter the measured properties of pRFs. In particular, the fMRI response of a voxel may be driven by different groups of cells depending upon the properties of the stimulus. While most studies have used simple luminance-defined stimuli (such as checkerboards) to generate pRF maps, more complex stimuli may be especially suited for generating maps in higher visual areas (**Yildirim et al., 2018**). A recent study that used a pRF mapping stimulus designed specifically to isolate orientation contrast showed reductions in measured pRF size in higher visual areas such as LO compared to the measurements made with standard luminance-based stimuli (**Yildirim et al., 2018**). pRF sizes have also been shown to vary based on whether the stimulus used allowed the contribution of contour integration mechanisms or not (**Dumoulin et al., 2014**). In the motion domain, there is evidence that MT+ may be more susceptible to stimulus configuration than earlier visual areas (**Alvarez et al., 2015**) but to date there has been no systematic investigation of the effects of different motion stimuli on pRF measurement.

Given the above variations due to stimulus properties and attentional state, in this study we asked whether stimuli thought to preferentially drive distinct stages of the motion-processing hierarchy can similarly alter the estimation of pRF parameters. In our initial experiment, we tested this with a moving bar stimulus similar to those commonly used in pRF mapping studies, defined by dots moving coherently. We then used different backgrounds in an attempt to differentially drive responses in different brain regions. In the bar-only condition, there was no background and the bar was presented alone. We predicted that this stimulus would generate a strong visual signal and enable the generation of pRF maps at all levels of the motion-processing hierarchy, much like a typical pRF mapping stimulus. In the 'kinetic' condition the bar was defined by kinetic boundaries. We predicted that if these stimuli are preferentially processed in KO/V3B, we might expect smaller pRF sizes and a higher proportion of voxels responding in this area. Finally, in the 'global' condition, the background consisted of incoherently moving dots. Here, higher visual areas that process stimuli in a more global manner should be able to distinguish between the bar and background and thus generate good pRF maps. In contrast, for these latter two conditions, we predicted that V1 would not be able to distinguish the bar from the background, leading to a reduced response.

In a second experiment, we asked whether any differential responses seen in the first experiment were a consequence of differences in the selectivity of these motion-selective regions, or could be explained by other factors, such as the visibility of the stimulus. We compared a bar-only stimulus to

two conditions with lower visibility bars: one motion-defined stimulus, where the bar was defined by transparent motion (against a non-transparent background), and a non-motion defined stimulus, where the bar was instead defined by differences in dot size. We predicted that if the responses were due to differential motion processing, we should see a different pattern of responses to these two stimuli: for example, the ‘transparent’ stimulus should show lower responsivity than the ‘size defined’ stimulus in V1, but higher responsivity in higher visual areas selective for global motion. In a similar vein, the subtle dot size difference in the size-defined stimulus should maximize the signal in V1 and the early visual cortex compared to higher regions. However, if the responses are simply due to the visibility of the bar stimulus, we predict similar responses for the two conditions across different visual areas.

## **2. Experiment 1**

Here we examined retinotopic maps and pRF properties across the visual hierarchy using three distinct mapping stimuli: the ‘bar-only’ stimulus, similar to standard retinotopic mapping stimuli; the ‘global’ bar stimulus with coherent motion against a background of noise; and the ‘kinetic’ bar stimulus with coherent motion against a background of oppositely-moving dots.

### **2.1. Materials and Methods**

#### *2.1.1. Participants*

Five participants (one male) took part in Experiment 1, including two of the authors (AH and JG) and three experienced participants naïve to the aims of the study. Participants were aged between 24-36 years (mean = 29.6 years) and one participant was left handed. All participants were experienced in an fMRI context and had normal or corrected-to-normal visual acuity. Written consent was acquired from all participants to ensure that they understood the potential risks associated with fMRI. The experiments were approved by the UCL Research Ethics Committee.

#### *2.1.2. Stimuli*

Figure 1 shows a schematic of the experimental set up, and GIF versions of the different experimental stimuli are available as supplementary material.

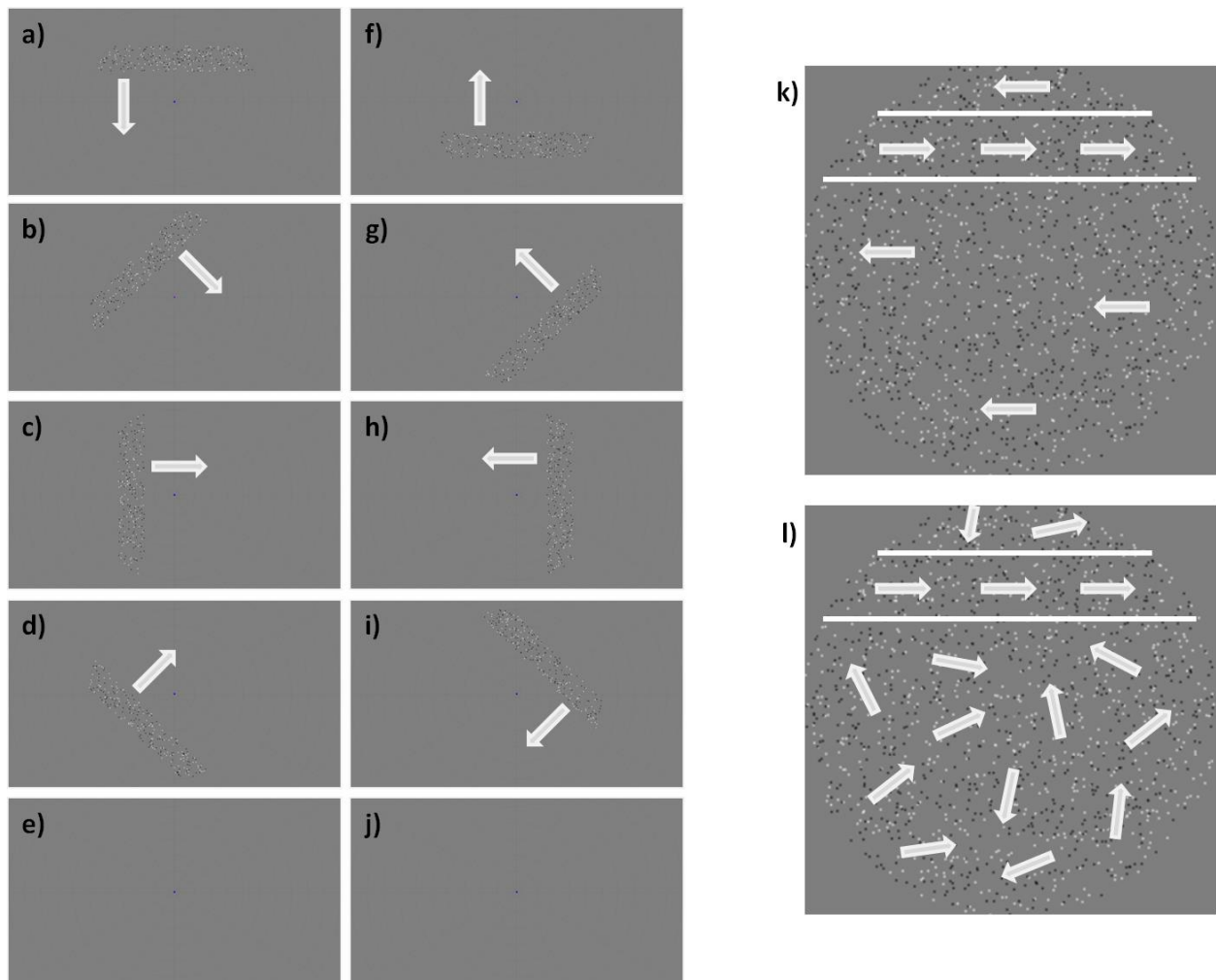


**Figure 1.** Schematic diagrams of the experimental set up in Experiment 1. (a) to (j) show one experimental run for the 'bar-only' condition, in the trial order presentation used for all stimuli in Experiment 1. Arrows indicate the direction of movement of the bar. Note in (b) that the fixation dot has changed colour, as part of the attentional task used in the experiment. (k) shows a schematic of the 'kinetic' condition. Within the bar (the area within the white lines) the dots moved in one direction (orthogonal to the bar movement); outside this area, they moved in the opposite direction. (l) shows a schematic of the 'global' condition; the movement inside the bar is in one direction, but outside the bar, the dots move in random directions.

Stimuli were created using MATLAB (MathWorks, Natick, MA) and the Psychophysics toolbox (Brainard, 1997; Pelli, 1997). Stimuli were projected onto a screen (resolution 1920 x 1080 pixels, size 36.8 x 20.2cm) at the rear of the scanner bore, with the screen image reflected off a mirror attached above the head coil. The viewing distance was 67cm, meaning the screen subtended 30.7 x 17.1 degrees of visual angle on the retina. The refresh rate was 60Hz.

The experimental stimulus consisted of a field of 2000 dots (diameter = 0.09°) against a uniform median grey field. Half of the dots were randomly selected to be white, and the other half were black. The initial positions of the dots were randomly determined within a rectangular aperture 16 x 16° in size. A mask was then applied to the image, such that only the dots within a circle with 8°

radius from the centre of the screen could be seen. A smaller circular mask (diameter =  $0.8^\circ$ ) was also applied at the fixation point (diameter =  $0.17^\circ$ ) to hide dots in this area and thus aid participants in maintaining their fixation. Further masks were also applied depending upon condition (see below). To further aid fixation, a low contrast “radar screen” pattern was shown behind stimuli (12 radial lines spaced 30 polar degrees apart, extending from just outside the fixation dot to the edge of the screen,  $15.5^\circ$ ), along with 11 concentric rings centred on fixation increasing in radius in equal steps of  $3^\circ$ .

A ‘bar’ was defined as a strip within the circular stimulus region that was  $2.4^\circ$  wide and up to  $16^\circ$  in length (the total width of the hidden stimulus rectangle). This area was shifted over the course of each trial in 25 discrete steps of  $0.7^\circ$  and 1 second each, beginning at one edge of the stimulus aperture and ending on the opposite side. The bar could be rotated to start in any one of the four cardinal directions or the four oblique directions, giving eight different trial types. In one run, all eight different trial types were presented, along with two null trials where no bar was present. The null trials were always presented as the 5<sup>th</sup> and 10<sup>th</sup> trials. The order of the other directions was fixed for all participants and went anticlockwise from the first direction, which was where the bar was horizontal, starting at the top of the screen and moving downwards.

There were three different stimulus conditions that could be presented in a given run to the participants. In each condition, the dots within the bar always moved in the same way; what differed between conditions was the movement of dots outside the bar area.

In the ‘bar-only’ condition, only the dots within the bar were visible, and therefore the bar appeared to be moving across a grey background. In the ‘kinetic’ condition, the dots outside the bar (within the circular stimulus region) were moving in the opposite direction to the dots within the bar at all times, creating a ‘shearing’ effect which made the bar visible. In the ‘global’ condition, the dots outside the bar moved in random directions, allowing the bar to be detected as a coherent global-motion stimulus. When a dot moved into the bar area (either through its normal progression or through a shift of the bar region), it started to move in the same coherent direction as all other bar dots. Similarly, when a dot left the bar area, it began to move randomly again. In all conditions, the null trials (with no bar present) had the same background motion as during the bar trials; a blank screen for the ‘bar-only’ condition, coherent motion in the ‘kinetic’ condition and random motion in the ‘global’ condition.



In all conditions, dots within the bar all moved in the same direction and moved along the length of the bar (so if the bar was moving from the top to the bottom of the screen, the dots moved from left to right or vice versa). All the dots (in both bar and background) changed direction by 180 degrees every 0.5 seconds, to prevent adaptation to one motion direction. Dots moved at  $0.8^\circ/\text{second}$  in all conditions. If any dots moved outside the aperture during the experiment, they were moved back one aperture width in the appropriate direction.

Each trial took 25 seconds, meaning that a run took 250 seconds/4 minutes and 10 seconds (plus a short period at the beginning of the run that was used to ensure that the fMRI signal had reached equilibrium). Each participant completed 4 runs for each condition, giving a total of 12 runs in the entire experiment. The order of the different conditions varied for different participants to control for order effects.

### *2.1.3. Fixation task*

Participants were instructed to focus on a blue fixation dot (diameter =  $0.17^\circ$ ) at all times and to press a button on an MRI-compatible button box when they saw it change colour (to a red-purple). The probability of the blue dot changing colour was 0.01 every 200ms and the colour change periods lasted 200 ms each. The results of this attentional task were unrecorded, and simply served to keep the participant fixated and alert throughout the experiment. An eye tracker (Eyelink 1000, sampling at the screen refresh rate of 60Hz) was used to monitor eye movements and ensure that participants were fixating correctly. We determined gaze stability using the methods outlined in **(Haas and Schwarzkopf, 2018)**; briefly, this involves calculating the median absolute deviation of the sampled gaze positions along both the horizontal and vertical dimensions for each run, and using these measures to compare the stability of gaze across conditions. Any run where fewer than 10 valid samples were taken was removed from further analysis. One participant was not eye tracked during either experiment, and therefore eye tracking data reflects the average of four participants in both Experiments 1 and 2. Analysis of the difference in eye position between conditions (both in the x and y directions) used general linear mixed models (using condition as a fixed factor, and subject and repeat number as random factors) followed by posthoc pairwise comparisons, with packages lme4 **(Bates et al., 2014)** and emmeans **(Russell, 2018)** in R (version 3.5.0).

### *2.1.4. Data acquisition*

Scans were acquired using a Siemens Avanto 1.5T MRI scanner with a 32-channel Siemens head coil located at the Birkbeck-UCL Centre for Neuroimaging. We used a modified version of the head coil



without the eye visor to allow an unrestricted view of the screen, leaving 30 effective channels. We used functional T2\*-weighted multiband 2D echo planar imaging with a multiband sequence (Breuer et al., 2005) (voxel size = 2.3mm isotropic, field of view = 96 x 96, 36 slices, repetition time (TR) = 1s, echo time (TE) = 55ms, flip angle = 75°, acceleration factor = 4). We collected 260-262 volumes (depending on stimulus condition) per run, and 4 runs were collected per condition for each participant. We also acquired a T1-weighted anatomical magnetisation-prepared rapid acquisition with gradient echo (MPRAGE) scan for each participant (TR = 2730ms, TE = 3.57ms) with a resolution of 1mm isotropic voxels.

### 2.1.5. Analysis

The method used for analysing pRFs has been described previously (Alvarez et al., 2015; Dumoulin and Wandell, 2008; Moutsiana et al., 2016; Schwarzkopf et al., 2014; van Dijk et al., 2016). In brief, the SamSrf MATLAB toolbox (available at <http://dx.doi.org/10.6084/m9.figshare.1344765>) models the pRF of each voxel as a 2D Gaussian in the visual field, incorporating a canonical haemodynamic response function based on the average of 26 participants in a previous study (Haas et al., 2014). For each voxel the model finds the best-fitting visual field location, spread (standard deviation), and overall response amplitude of the pRF function.

Preprocessing of the fMRI data was carried out using SPM12 (Wellcome Centre for Human Neuroimaging, London, <http://www.fil.ion.ucl.ac.uk/spm/software/spm12/>). The first 10-12 volumes (depending on stimulus condition) were removed to allow the signal to reach equilibrium, leaving 250 volumes to be used in analysis for all participants and conditions. We then carried out intensity bias correction, realignment, unwarping and coregistration of the functional data to the structural scan, all using the default parameters built into the SPM software. FreeSurfer (<https://surfer.nmr.mgh.harvard.edu/fswiki>) was used to generate a 3D reconstruction of the grey-white matter surface (Dale et al., 1999; Fischl et al., 1999), and the functional data was then projected to the cortical surface. Linear detrending was applied to the time series from each vertex in each run, and runs of the same stimulus condition were z-standardised and averaged together.

Population receptive field analysis was carried out on the occipital lobe data in a two-stage procedure. With a binary aperture describing the position of the bar element within each stimulus for each scanning volume, we calculated its overlap with a profile of a pRF to predict the fMRI time series in the experiment. We first carried out a coarse grid search fit on data smoothed with a large kernel on the spherical surface (full width half maximum = 5), allowing calculation of the three pRF

parameters that gave the maximal Pearson's correlation between the predicted and observed time series for the full set of search grid parameters and vertices. These parameters were then used to seed an optimisation algorithm (**Lagarias et al., 1998; Nelder and Mead, 1965**) in a slow fine fit procedure on a vertex by vertex basis using unsmoothed data, allowing refinement of the parameter estimates and the calculation of an estimate of response strength.

Visual areas V1, V2 (dorsal and ventral), V3 (dorsal and ventral), V3A, V3B and MT+ (defined as TO1 and TO2) were delineated based on reversals in the polar angle map from the 'bar-only' stimulus condition (for participants who only completed Experiment 2, the 'transparent bar-only' condition was used instead) (**Sereno et al., 1995**). These regions can be seen in Figure 2.

## 2.2. Results and Discussion

### 2.2.1 Relationships between maps

Figure 2 shows the left hemisphere polar angle maps for each experimental condition and each participant in Experiment 1 ( $R^2$  threshold = 0.05). Visual inspection of these images suggests that the 'bar-only' condition (Figure 2A) produces the clearest polar angle maps across participants, while the 'kinetic' condition (Figure 2B) tends to show a similar, if weaker pattern. The 'global' stimulus (Figure 2C) shows a weaker response still, with lower visual areas (e.g. V1) showing very little response. Although we had a relatively small number of participants, these general trends are highly consistent.

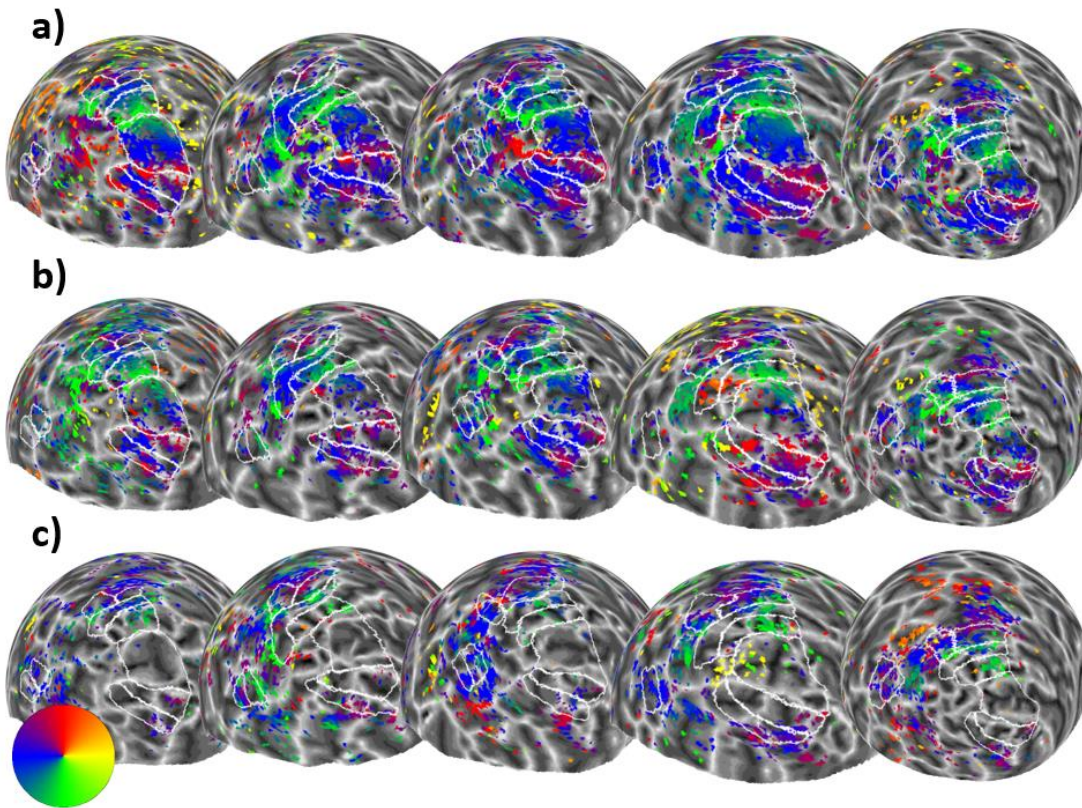


**Figure 2.** Sphere projection of polar angle data for the left hemispheres of all participants in Experiment 1. The colour of each vertex indicates the polar angle for the corresponding pRF centre (as indicated by the colour wheel). Each person's data forms a column, and stimulus condition forms a row. Manual delineations of visual areas V1, V2, V3, V3A, V3B and TO1/2 are shown. (a) Polar angle estimates for the 'bar-only' stimulus condition. (b) Polar angle estimates for the 'kinetic' stimulus condition. (c) Polar angle estimates for the 'global' stimulus condition.

We determined the proportion of vertices within each of these visual areas responding retinotopically in the three experimental conditions (goodness of fit of the pRF model  $R^2 > 0.05$ , Figure 3A). The bar stimulus produced the biggest response in areas V1-V3, which then dropped off for the higher visual areas (V3A, V3B and MT+). In contrast, responses to the kinetic stimulus increased across areas V1-V3, levelling off at V3A-V3B and then dropping in MT+. Responses to the global stimulus were even lower in the early visual areas, but again increased, reaching a peak at V3A and V3B. There were therefore large differences in stimulus responsivity in V1-V3, but these differences were much reduced in the higher visual areas. There was a significant interaction between condition and visual area in the final model of the data (interaction:  $\chi^2 = 336.06$ ,  $p < 0.001$ ; main effect of visual area:  $\chi^2 = 141.63$ ,  $p < 0.001$ ; main effect of condition:  $\chi^2 = 377.49$ ,  $p < 0.001$ ).

Comparing the goodness of fit across conditions (Figure 3B) showed a similar pattern, with initially large differences in  $R^2$  in the early visual areas that again decreased in higher regions. This interaction between condition and visual area was again significant (interaction:  $\chi^2 = 60.629$ ,  $p < 0.001$ ).

0.001; main effect of visual area:  $\chi^2 = 62.747$ ,  $p < 0.001$ ; main effect of condition:  $\chi^2 = 242.912$ ,  $p < 0.001$ ). The area with the highest average  $R^2$  value also differed for each condition; the peak was in V3 for the bar stimulus, V3A for the kinetic stimulus and V3B for the global stimulus.

Finally, we analysed the pRF size across conditions and visual areas (Figure 3C). Mean pRF sizes were smallest in the early visual areas, V1-V3, increasing in higher regions. pRFs were also relatively similar in early visual areas for all three conditions, but clear differences emerged in V3A, V3B and MT+. Here, pRFs were largest for the bar condition, smaller for the kinetic condition, and smaller again for the global condition (though in all cases larger than the equivalent condition in earlier regions). Again, there was a significant interaction between condition and visual area (interaction:  $\chi^2 = 47.879$ ,  $p < 0.001$ ; main effect of visual area:  $\chi^2 = 174.505$ ,  $p < 0.001$ ; main effect of condition:  $\chi^2 = 24.434$ ,  $p < 0.001$ ).

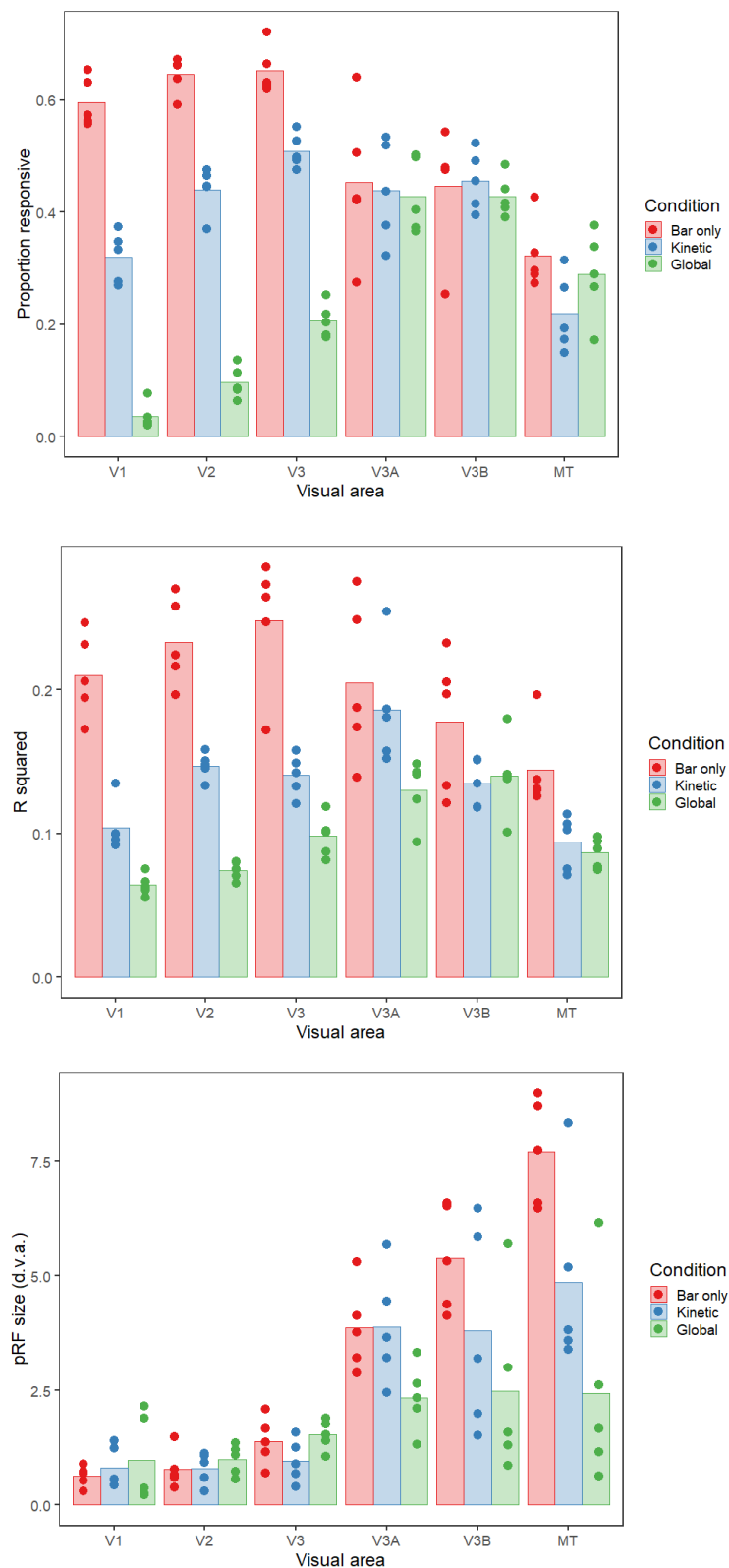


**Figure 3. (a)** Proportion of vertices responding, **(b)** goodness-of-fit and **(c)** pRF sizes for each condition and visual area in Experiment 1. The bars show the mean values across all subjects, and the points are individual data for each subject. In (a), this is the mean proportion of vertices responding for each subject, whereas for (b) and (c) these are the median goodness-of-fit values and pRF sizes respectively.

## 2.2.2 Control analyses

As there were clear differences in the proportion of responsive voxels in the three conditions, it is possible that the differences in pRF size between conditions were due to this reduction in the voxels included in each analysis, rather than a specific change in pRF size within each voxel. To examine this possibility, we analysed the data for the ‘bar-only’ condition using just the voxels that survived thresholding for the kinetic and global conditions (see Figure 4). The pattern of results is similar to Figure 3C – pRF sizes were again comparable in early visual areas for the three conditions, with clear reductions in pRF size for the kinetic and global conditions in areas V3A, V3B and MT+. In this case however, the reduction can be attributed to the differential selection of voxels responding to the same stimulus. In other words, the observed pRF size differences in Figure 3C are likely due to changes in the voxels that respond to these stimuli rather than active changes in pRF size across the different conditions. Using a linear model to compare the kinetic and global vertex conditions from the control analysis with the kinetic and global data in the original analysis showed no significant difference between the two data sets ( $\chi^2 = 0.758$ ,  $p = 0.384$ ).

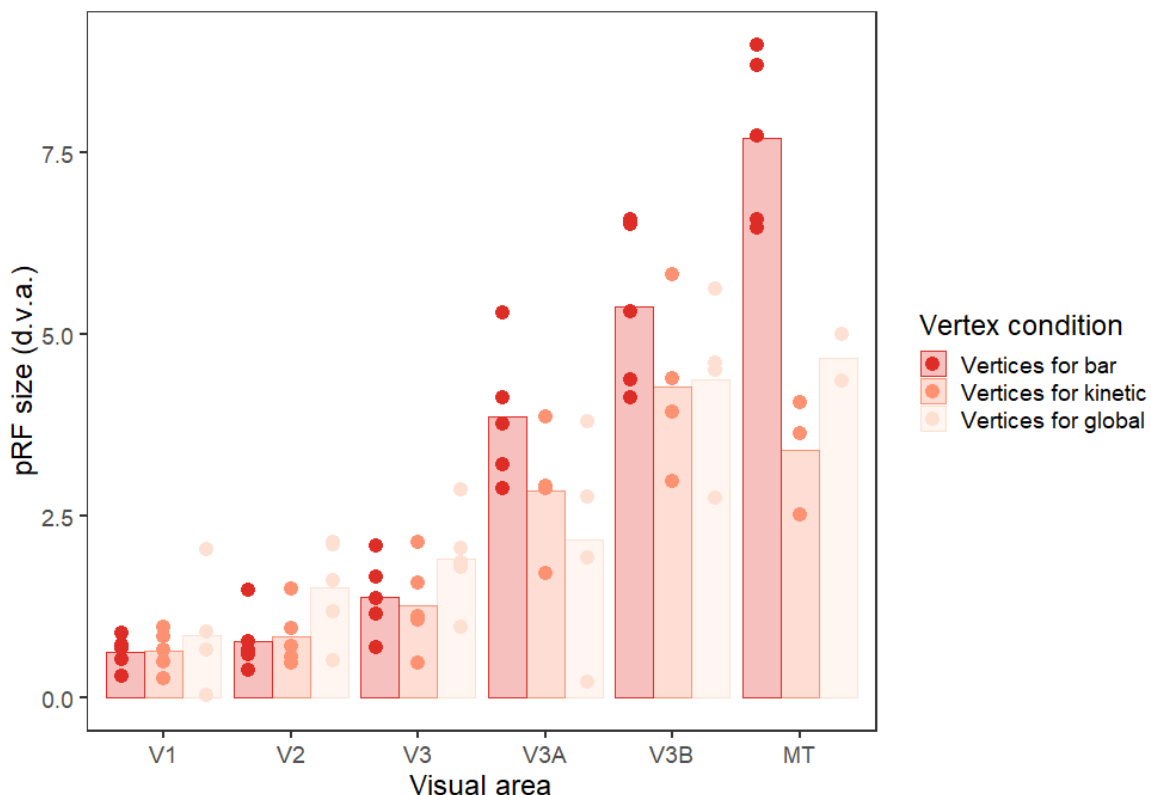


**Figure 4.** Plot to show pRF sizes for each visual area in Experiment 1 for the bar-only condition, using the responsive vertices for all three conditions. The bars show the mean values across all subjects, and the points are individual data for each subject (median pRF sizes). Any data points with a value of zero (obtained if the vertices for the condition do not overlap with any bar activation) were removed before plotting, leading to unequal numbers of data points in each condition.

It is also possible that differences between conditions could be attributed to differences in fixation stability between conditions. However, a second control analysis showed that the mean of the median absolute deviations of eye position was highly consistent and relatively low for both horizontal and vertical eye movements, averaging less than 0.5 degrees of visual angle for every condition (see Figure 5). General linear mixed models followed by posthoc pairwise comparisons suggested that there were no significant differences in eye position between conditions, either for the X or the Y direction (for X, bar-kinetic:  $t_{30.14} = 0.356$ ,  $p = 0.933$ , bar-global:  $t_{30.26} = 0.457$ ,  $p = 0.892$ , kinetic-global:  $t_{30.35} = 0.101$ ,  $p = 0.994$ . For Y, bar-kinetic:  $t_{30.35} = -0.614$ ,  $p = 0.814$ , bar-global:  $t_{30.14} = -0.503$ ,  $p = 0.871$ , kinetic-global:  $t_{30.43} = 0.111$ ,  $p = 0.993$ ).

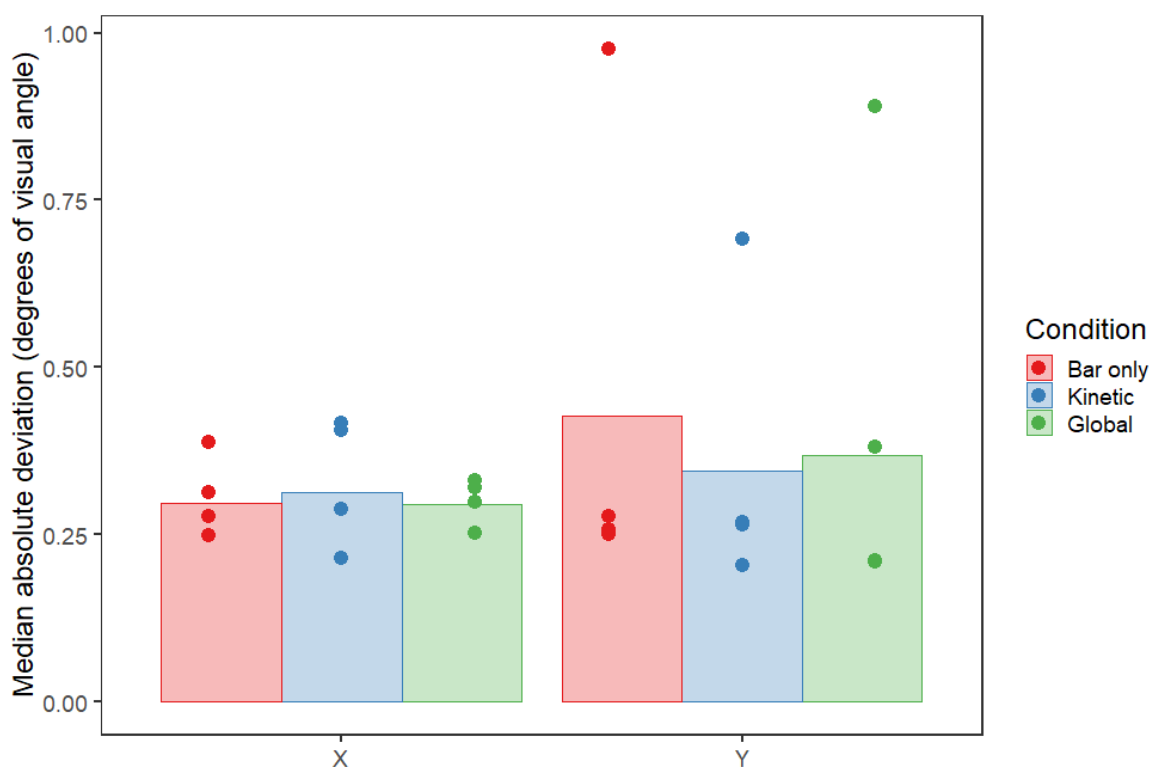


**Figure 5.** Plot showing the mean of the median absolute deviation of eye position across runs, conditions and observers ( $n = 4$ ) for both the X (horizontal) and Y (vertical) dimensions of Experiment 1, in degrees of visual angle. Error bars are  $\pm 1$ SD of the mean.

### 2.2.3 Experiment 1 summary

Altogether, the three stimulus types (bar-only, kinetic, and global) produced clear differences in responsivity, goodness-of-fit, and pRF size across the visual hierarchy. Our control analyses reveal that these differences cannot be attributed to differences in gaze stability between the conditions and that the observed differences in pRF size are unlikely to reflect stimulus-driven changes in pRF



size within each voxel. Rather, it seems likely that the observed differences in pRF size can be attributed to responses from different sub-populations of voxels in the three different conditions. We next turn our attention to the source of the differences in responsivity that appear to be driving these differences in pRF size. In particular, it is possible that differences in the visibility or salience of the bar between these conditions could drive the differences in responsivity. We explore this possibility in Experiment 2.

### 3. Experiment 2

As outlined in the introduction, estimates of pRF size and visual field location have been found to vary according to both the properties of the mapping stimulus and the attentional state of the observer. Although it is tempting to attribute the differences observed in Experiment 1 to differences in the effectiveness of these stimuli at driving the selectivity of various stages of the motion-processing hierarchy, the visibility of the bar element in each stimulus also varied substantially between the three conditions. Most participants in Experiment 1 informally noted that the bar was less clear in the global condition than in the kinetic or bar-only conditions. It is possible then that the differences observed were driven by the visibility or salience of the bar, rather than any difference in the underlying selectivity of the motion detectors in each brain region.

In Experiment 2 we sought to test this by comparing the bar-only stimulus with two new stimuli. Firstly, we devised a second form of stimulus defined by global motion, a ‘transparent’ stimulus where the bar contained two sets of dots moving in opposite directions to give the appearance of two sheets moving transparently across each other (**Snowden and Verstraten, 1999**). The global percept of these two directions requires an integration across space that is similar to that for a single direction of global motion amongst noise (**Edwards and Greenwood, 2005; Edwards and Nishida, 1999**). Transparent motion is not perceived when dots with opposing directions are ‘locally balanced’ within small regions of the visual field (**Qian et al., 1994**), perhaps due to an intermediate process of ‘local-motion pooling’ prior to the global-motion stage (**Edwards et al., 2012; Vidnyánszky et al., 2002**). Although the responses of V1 neurons cannot distinguish between transparent and non-transparent stimuli, both fMRI (**Muckli et al., 2002**) and electrophysiological studies (**Qian and Andersen, 1994; Snowden et al., 1991**) show a differential response within MT/V5. Transparent-motion stimuli thus offer another stimulus with which we can assess whether pRF parameters differ when stimuli preferentially drive higher levels of the motion-processing hierarchy. We therefore constructed bar stimuli with two opposing directions of transparent motion within the bar, presented against a background of locally-balanced dots that do not appear transparent. If the differences in pRF parameters found in Experiment 1 are due to differences in

motion selectivity, we would expect the transparent-motion bar stimulus to produce weaker responses in lower visual areas and a reduction in pRF size in higher visual areas, as with the ‘global’ condition.

Our second comparison stimulus was intended to examine the role of stimulus visibility in these effects. Transparent motion in particular has been found to be less visible in peripheral vision than in the fovea (**De Bruyn, 1997**), which would likely create issues for the visibility of our transparent bar stimuli as they traverse the visual field, just as it may have been an issue in Experiment 1. We therefore compared these transparent stimuli with a stimulus bar that was not defined by differences in motion, but rather by a subtle difference in stimulus dot size. This bar stimulus would likely differentially drive the responses of early visual areas, given their potential role in the perception of object size (**Moutsiana et al., 2016; Murray et al., 2006; Pooresmaeili et al., 2013; Sperandio et al., 2012**), but should not differentially drive the responses of higher motion-selective regions as effectively as the motion-defined bars used previously. The size difference in these stimuli does however lead to a substantial reduction in the visibility of the bar stimulus relative to the bar-only condition, particularly in peripheral vision. In particular, we selected a size difference that produced a similar level of subjective visibility to the ‘transparent’ condition (examined during pilot testing). Were this size-defined condition to produce similar responses to the motion-defined condition, this would suggest that visibility or salience is a more likely explanation for the observed differences than the stimulus selectivity of the underlying neural populations.

### **3.1. Materials and Methods**

#### *3.1.1. Participants*

Five participants (two male) took part in Experiment 2, including all four authors and one non-author participant from the first experiment (age range 28-39 years, mean age: 32.6 years). One participant was left handed. All had normal or corrected-to-normal visual acuity and provided written consent, as in Experiment 1.

#### *3.1.2. Stimuli*

The second experiment was set up with the same apparatus and general stimulus properties as the first. Here there were three conditions related to the mapping stimuli: ‘bar-only’, ‘transparent’ and ‘size-defined’. The ‘bar-only’ condition in this experiment was identical to the ‘bar-only’ condition in Experiment 1, except that the dots were paired such that two dots were always yoked together such that both dots in the pair travelled in the same direction. However, different pairs travelled in orthogonal directions. This created the impression of two ‘sheets’ of dots travelling over each other

in opposite directions. As in the 'bar-only' condition of Experiment 1, the null trials for this condition contained only the uniform grey background. The speed of the dots was reduced in this condition to 0.34°/second to increase the impression of transparency.

In the 'transparent' condition, the bar was identical to the bar in the 'bar-only' condition. In this case however, the background also contained paired dots, with each dot in the pair moving in opposite directions, leading to the perception of non-transparent motion (as with 'locally paired' dot stimuli used previously (Qian et al., 1994)). To keep dots within these local regions and avoid them unpairing over time, the motion of the dots periodically reversed. The timing of these reversals was randomised across dot pairs, so that reversals did not occur for all of the dots at the same time, a feature that enhances the percept of transparent sheets moving across one another (Kanai et al., 2004) when dot trajectories are limited (though not when locally paired, as in the background). The consistent pairing of dots between bar and background (differing only in their consistent vs opposing directions) meant that bar and background did not differ in dot density, and that the only feature to distinguish the bar was the percept of transparency against a background of non-transparent flicker.

The 'size-defined' condition contained a bar that was defined by a difference in dot size rather than by motion type; the dots in the bar were 0.10° in diameter against a background of dots with 0.09° diameter. All the dots in this condition moved in random directions, though with the same frequency of direction reversal as in the other two conditions (i.e. dots oscillated back-and-forth along a randomly selected axis). Null trials for this condition were the same as for the 'global' condition in Experiment 1.

To minimize anticipation effects in this experiment, the starting orientation and direction of the sequence (anticlockwise or clockwise shifts) was randomised for each condition and participant, but kept constant across the four runs. Note that this meant that the movement direction of the bar always changed in a sequential fashion. All other presentation and analysis procedures were as in Experiment 1.

## 3.2. Results and Discussion

### 3.2.1 Relationships between maps

As in Experiment 1, the bar-only stimulus produced clear and consistent polar maps across participants (Figure 6A). However, the transparent and size-defined stimuli produced much weaker and more variable maps (Figure 6B & C), particularly in lower visual areas (e.g. V1) where responses

were considerably reduced. Interestingly, participants who self-reported that they were frequently unable to detect the the transparency or size-defined bar stimuli (shown by red crosses in Figure 6) also had virtually no discernable map structure for these conditions.

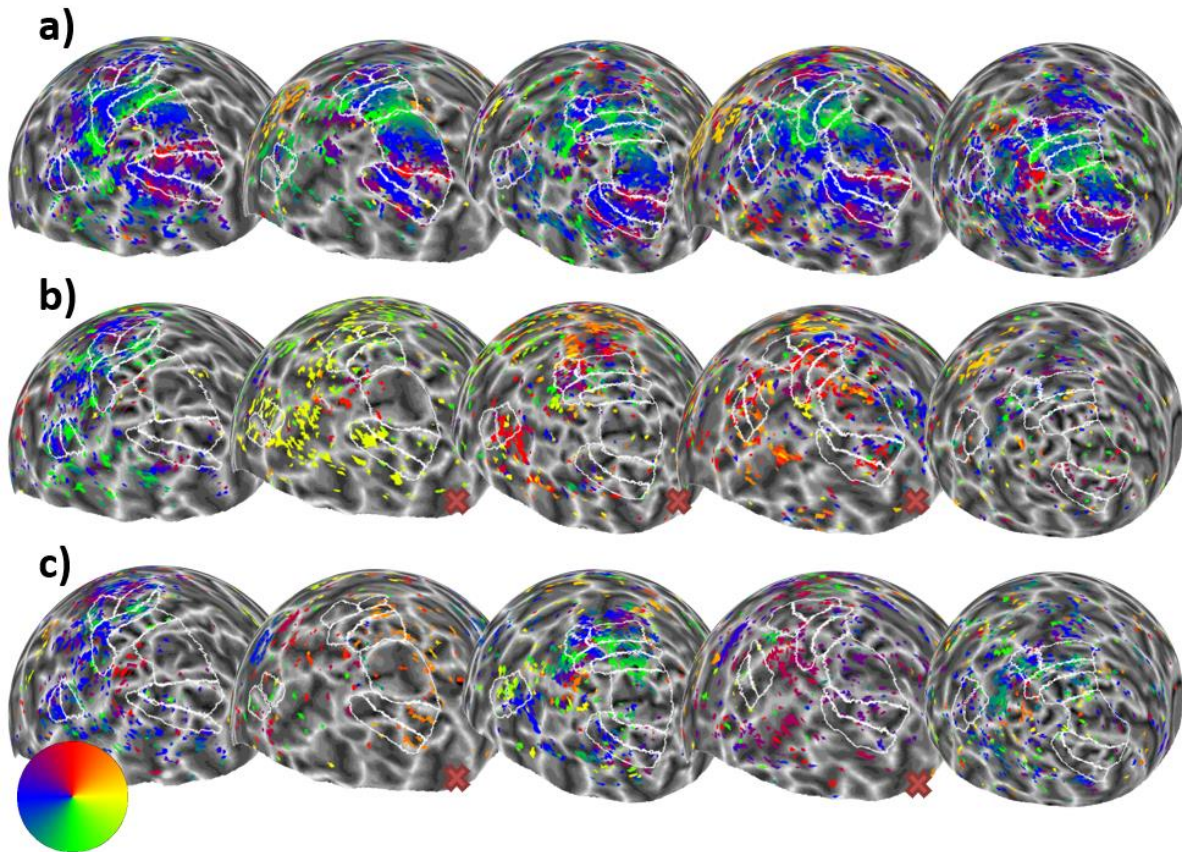


**Figure 6.** Sphere projection of polar angle data for the left hemispheres of all participants in Experiment 2. The colour of each vertex indicates the polar angle for the corresponding pRF centre (as indicated by the colour wheel). Each person's data forms a column, and stimulus condition forms a row. Manual delineations of visual areas V1, V2, V3, V3A, V3B, and TO1/2 are shown (if the subject had taken part in Experiment 1, the delineations from this experiment were used). (a) Polar angle estimates for the 'bar-only' stimulus condition. (b) Polar angle estimates for the 'transparent' stimulus condition. (c) Polar angle estimates for the 'size-defined' stimulus condition. Red crosses indicate where participants self-reported low awareness of the stimulus when questioned after the experiment.

As in Experiment 1, we determined the proportion of vertices responding retinotopically in the different experimental conditions (see Figure 7A). Here, the bar-only condition produced similar response levels to the equivalent condition in Experiment 1, with these levels again decreasing in higher regions. In comparison, the transparent and size-defined conditions showed greatly reduced responsivity in early visual areas, similar to the global condition in Experiment 1. Responsivity in these conditions increased in later visual areas, though not quite to the level of the bar-only stimulus (unlike the global condition). There was a significant interaction between condition and visual area in the final model (interaction:  $\chi^2 = 52.330$ ,  $p < 0.001$ ; main effect of visual area:  $\chi^2 = 24.933$ ,  $p < 0.001$ ; main effect of condition:  $\chi^2 = 223.071$ ,  $p < 0.001$ ).

Similarly, the bar-only stimulus had much better goodness of fit compared to the transparent and size-defined stimuli, matching the pattern observed in Experiment 1. Goodness of fit was also worst in V1 and MT for all conditions, with  $R^2$  values increasing for more intermediate visual areas (Figure 7B). Modelling of the goodness of fit showed that there was no significant interaction between condition and visual area, ( $\chi^2 = 16.505$ ,  $p = 0.086$ ). However, there were significant main effects of visual area ( $\chi^2 = 30.060$ ,  $p < 0.001$ ) and condition ( $\chi^2 = 289.304$ ,  $p < 0.001$ ).

Finally, we considered differences in pRF size for the different conditions and visual areas (Figure 7C). Again, as in Experiment 1 there was a highly significant interaction between condition and visual area (interaction:  $\chi^2 = 64.806$ ,  $p < 0.001$ ; main effect of visual area:  $\chi^2 = 72.031$ ,  $p < 0.001$ ; main effect of condition:  $\chi^2 = 21.572$ ,  $p < 0.001$ ). With the bar-only stimulus, pRF size increases dramatically across visual areas, with values comparable to those of Experiment 1. Although pRF values for the transparent and size-defined stimuli are comparable in early areas, the rate of increase is much lower than in the bar-only condition, resulting in considerably smaller pRFs in the highest areas. In MT these values were broadly comparable to the global condition of Experiment 1 for the size-defined stimulus, though generally much smaller for the transparent stimulus.

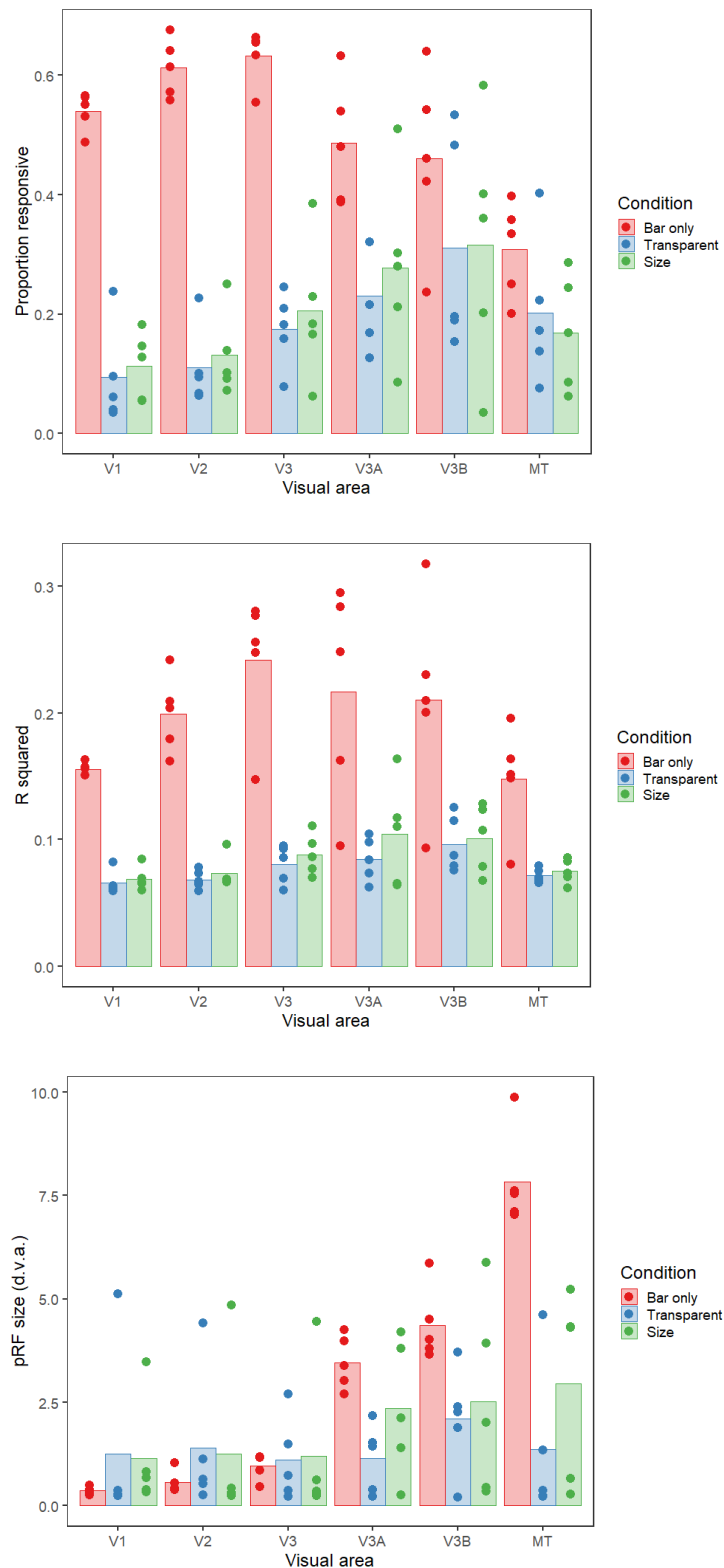


**Figure 7. (a)** Proportion of vertices responding, **(b)** goodness-of-fit and **(c)** pRF sizes for each condition (bar-only, transparent, and size-defined) and visual area in Experiment 2. The bars show the mean values across all subjects, and the points are individual data for each subject. In (a), this is the mean proportion of vertices responding for each subject, whereas for (b) and (c) these are the median goodness-of-fit values and pRF sizes respectively.



### 3.2.2 Control analyses

As in Experiment 1, a control analysis was run to examine whether the above differences in pRF size between conditions were due to this reduction in the voxels included in each analysis. We again analysed data for the bar-only condition using just the voxels that survived thresholding for the transparent and size-defined conditions. This again produced a clear reduction in pRF size for these two conditions in areas V3A, V3B and MT, suggesting that the observed differences in pRF size may be predominantly explained by differences in the responsivity of voxels (Figure 8). This is supported by statistical analysis suggesting that there is no significant difference between the transparent and size-defined conditions in the control analysis and in the original experimental analysis ( $\chi^2 = 0.111$ ,  $p = 0.739$ ).

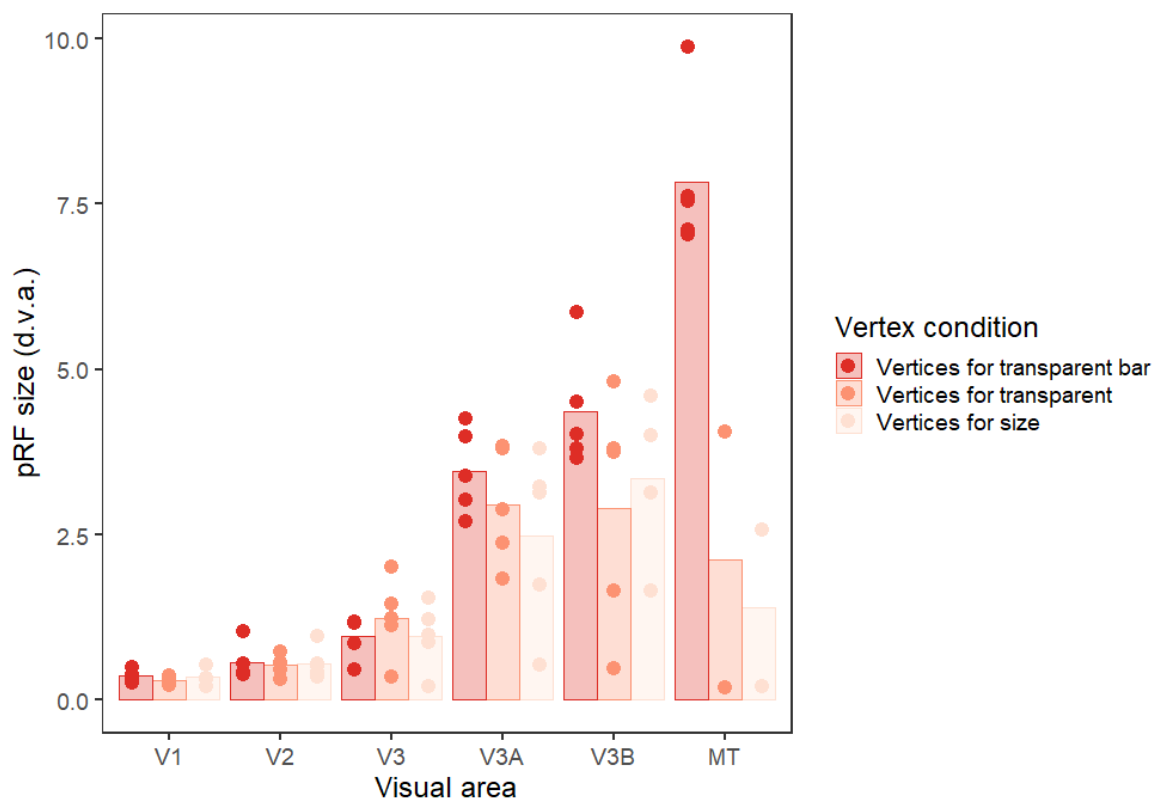


**Figure 8.** Plot to show pRF sizes for each condition and visual area in Experiment 2 for the transparent bar-only condition, using the responsive vertices for all three conditions. The bars show the mean values across all subjects, and the points are individual data for each subject (median pRF sizes). Any data points with a value of zero (obtained if the vertices for the condition do not overlap with any bar activation) were removed before plotting, leading to unequal numbers of data points in each condition.

As in Experiment 1, the results of Experiment 2 also do not seem to depend on eye movements, as the mean of the median absolute deviations of eye position was highly consistent and relatively low for both horizontal and vertical eye movements, with averages of less than 0.5 degrees of visual



angle for both conditions (see Figure 9). General linear mixed models followed by posthoc pairwise comparisons suggested that there were no significant differences in eye position between the bar-only and size-defined conditions, either for the X or the Y direction (for X, bar-transparent:  $t_{35.20} = -0.055$ ,  $p = 0.998$ , bar-size:  $t_{35.04} = -1.439$ ,  $p = 0.332$ , transparent-size:  $t_{35.20} = -1.354$ ,  $p = 0.375$ . For Y, bar-transparent:  $t_{35.23} = 0.667$ ,  $p = 0.784$ , bar-size:  $t_{35.05} = -1.513$ ,  $p = 0.297$ , transparent-size:  $t_{35.23} = -2.149$ ,  $p = 0.094$ ). As before, this suggests that participants were highly compliant with the fixation instructions.

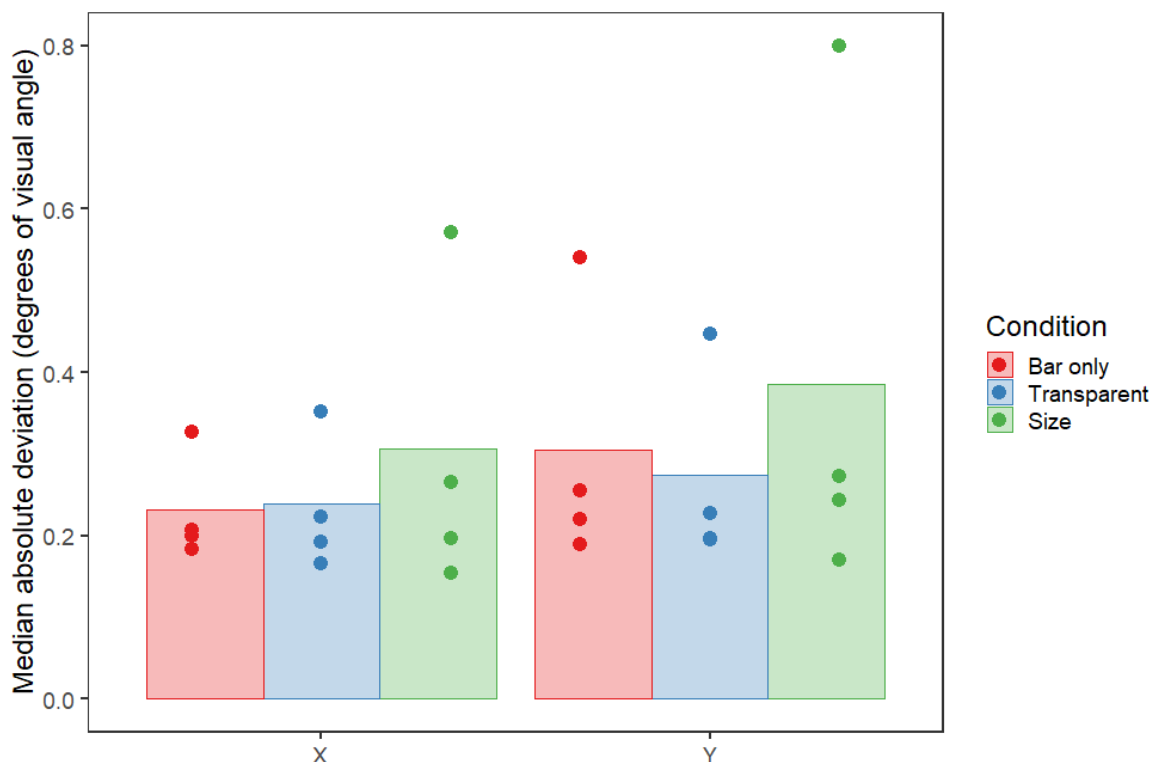


**Figure 9.** Plot showing the mean of the median absolute deviation of eye position across runs, conditions and observers ( $n = 4$ ) for both the X (horizontal) and Y (vertical) dimensions of Experiment 2, in degrees of visual angle. Error bars are  $\pm 1$ SD of the mean.

#### 4. Discussion

In this study, we show that retinotopic mapping stimuli defined by motion produce clear and highly consistent differences in the properties of population receptive fields (pRFs) measured across the visual hierarchy, including responsivity, goodness of fit, and pRF sizes. As predicted, we show that a bar mapping stimulus defined by moving dots (against a blank background) produces strong pRF maps in early visual areas, with responses dropping off and pRF sizes becoming larger in areas higher in the motion processing hierarchy. More complex motion stimuli, such as bars defined by kinetic

and global motion (against backgrounds of opposing motion or noise, respectively), produce a much lower degree of responsivity in early visual areas, with a reduction in pRF sizes for higher visual areas, and reductions in goodness of fit across the hierarchy as a whole. Control analyses further suggest that the reduction in pRF size can be attributed to the reduction in the voxels included for each stimulus, rather than changes in pRF size within voxels. Although it is tempting to attribute this to differences in the potential for these visual areas to distinguish these higher-order stimuli, a second experiment showed highly similar patterns of responsivity, goodness of fit, and pRF size across visual areas for a stimulus defined by transparent motion (against a non-transparent background) and a size-defined stimulus (with no differences in motion) that was matched in visibility. This suggests that the observed differences in pRF properties are not specific to mapping stimuli defined by differences in stimulus motion, and that they may instead reflect the visibility or salience of the stimulus.

As outlined in the introduction, evidence from a variety of experimental approaches suggests that motion is processed hierarchically in the visual system, with local motion processed in early visual areas, such as V1, and global motion processed in higher areas, such as MT+ (**Adelson and Movshon, 1982; Braddick et al., 2001; Van Essen and Gallant, 1994; Williams and Sekuler, 1984**). These differences in selectivity predict differences in pRF size and responsivity between local motion defined stimuli (such as our bar stimulus) and global motion defined stimuli (such as our global stimulus) for these different areas. Our results indeed show these differences, sometimes quite strikingly; the lack of response in V1 for the global stimulus is highly consistent across observers. Support for differences derived from other forms of motion selectivity is less clear. In particular, it has been suggested that kinetic boundary stimuli are processed preferentially in visual area V3B/KO (**Van Oostende et al., 1997**). However, our results show that responses were equally as strong in V3A, with comparable pRF sizes and goodness-of-fit values that were, if anything, better than V3B. Our results therefore suggest that although there were clear differences in the pRF properties measured in early visual areas with these stimuli, amongst higher areas these kinetic boundary stimuli produced widespread changes in pRF properties that are difficult to localize to any one area. This discrepancy compared with previous studies may well reflect the fact that delineating these areas is often controversial; there is still some debate about the exact location of KO, or indeed whether it can be considered a single, coherent visual area (**Larsson and Heeger, 2006**).

The fact that we see very similar response patterns for both our ‘transparent’ and ‘size-defined’ conditions in Experiment 2 further suggests that we should be cautious about attributing our results to differential motion processing in distinct visual areas. Instead, it seems more likely that the

variations in pRF parameters that we observe reflect the lower visibility of these stimuli relative to the more standard bar vs. blank background configuration. Part of this decrease in visibility could reflect the presentation of these bar mapping stimuli in peripheral vision. Our sensitivity to global motion (**Raymond, 1994**), transparent motion (**De Bruyn, 1997**), and kinetic boundaries or motion-defined form (**Regan and Beverley, 1984**) are all known to decline in the periphery. These declines can be corrected for by adjusting the contrast, size, and speed of stimuli (**Hess and Aaen-Stockdale, 2008; Regan and Hamstra, 1991**), at least to some extent. However, were the lack of eccentricity scaling a problem with our stimuli, we should have seen an increase in average pRF size with our motion-defined stimuli due to the loss of responsivity from neurons with small receptive fields (as seen in comparisons between size-invariant and eccentricity-scaled bar stimuli (**Alvarez et al., 2015**)). The decrease in pRFs that we observe suggests that the problem lies more with the detection of large receptive fields, though this may still reflect a suboptimal combination of contrast and/or speed for these large-field motion detectors. Participants certainly noted that the global and transparent conditions in particular were significantly less visible in peripheral vision, with those who reported particularly low visibility showing retinotopic maps that were far less structured than those who were better able to discern the bars (see Figure 6). Interestingly, similar results were seen in a retinotopic mapping study where the bars were defined by orientation contrast (**Yildirim et al., 2018**). In this case, a reduction in pRF size was seen when compared to a high contrast luminance retinotopic mapping stimulus, but not when a control low contrast luminance stimulus was used, at least in early visual areas. Small pRF estimates may thus be a general property associated with low-visibility mapping stimuli, including second-order bars, like those of the present study.

Visibility may also be an issue in the measurement of population receptive fields. These analyses rely on a difference in BOLD response when the stimulus bar and the background are presented in a given location of the visual field. Although unidirectional global motion typically drives BOLD responses in MT to a greater extent than incoherent noise (**Braddick et al., 2001**), incoherent noise stimuli still produce an increased response within MT relative to stationary stimuli (**McKeefry et al., 1997**). The same would be true for our kinetic boundary and transparent stimuli. It is possible therefore that the luminance-defined differences produced by the bar-only stimulus produce a clearer difference than the motion-defined differences of the other conditions, consistent with the observed reductions in goodness of fit for the pRF parameters derived using these motion-based stimuli. This could also explain why size-defined stimuli produced a similar pattern of results – these stimuli too would be expected to decrease the difference in BOLD response to the stimulus bar relative to the background. Larger pRF estimates are likely to be particularly vulnerable to this issue, given that these voxels tend to show the worst goodness-of-fit. For instance, in Experiment 1 there

was a clear negative correlation between  $R^2$  and pRF size in V1, even with the bar-only stimuli ( $\rho = -0.721$ ,  $p < 0.001$ ). Voxels with large pRF estimates may thus be the first to drop out with our motion-based stimuli, leading to our observed reductions in pRF size. Were this to be the case, our findings would in fact reflect the selectivity of visual brain regions for motion (given the increased responsivity to the stimulus background), though the reduction in pRFs could not be strictly interpreted as a property of the underlying neural populations.

Differences in attention to our peripheral stimuli could also play a role in our findings. Previous research has shown decreased responses in V1 (but stronger responses in parietal and frontal areas) when participants distinguished between stimulus and background entirely attentionally (**Saygin and Sereno, 2008**). While our stimuli were generally distinguishable visually (save for the participants who reported the transparent and size-defined stimuli as difficult to see), it is likely that the more complex second-order motion stimuli used in this experiment were more attentionally demanding than the 'bar-only' stimuli. Second-order motion has been found to be more difficult to process at multiple locations compared to first-order motion, suggesting that second-order motion is more attentionally demanding (**Lu et al., 2000**), and direction discrimination thresholds are influenced more strongly by attention for second-order motion compared to first-order motion (**Allen and Ledgeway, 2003**). This explanation implies that the attentional demands of the task are more important for determining the pRF responsivity and properties than the particular stimulus parameters.

A role for attention is also supported by other experiments. One recent study showed that it was possible to map retinotopic responses for bar stimuli defined by illusory contours, occluded parts of a bar, or very low luminance contrast (**Haas and Schwarzkopf, 2018**), suggesting that the mapping reflected spatial attention rather than specific visual properties of these stimuli. Similarly, while it has been shown that MT+ responses increase with the perception of a motion aftereffect, these responses can in fact largely be explained by the increased attention that subjects paid to the aftereffect stimulus compared to a control (**Huk et al., 2001**). While we also see pRF size reductions for higher visual areas in our study, the fact that we see them for stimuli defined by a number of different contrasts (motion and size) argues against this being a consequence of driving only neurons sensitive to a specific stimulus property. Instead, it suggests that pRFs could be measuring the attentional modulation rather than a visually responsive receptive field. We suggest that future studies should be carefully controlled for attentional confounds if they aim to test whether visual properties affect pRF size, as it may otherwise be difficult to interpret their results.

Another possibility is that our motion- and size-defined stimuli may have produced an illusory sense of depth for the bar stimulus, which may then have altered our measured pRF properties. It is known that areas such as V3B/KO and V3A are involved in the processing of depth cues (Tyler et al., 2006), and particularly with integration of depth cues with other signals, such as motion (Ban et al., 2012). However, we think this is unlikely to be a complete explanation of our results, as participants did not report strong depth percepts for any of our stimuli. In addition, it is not clear that this hypothesis would explain the patterns observed in our results; we did not see markedly stronger responses in V3A/V3B, as has been observed in previous fMRI studies of depth perception (Anzai and DeAngelis, 2010; Backus et al., 2001; Tsao et al., 2003). A related suggestion is that the responses in higher visual areas may be a consequence of surface segmentation cues; however, again, research has shown that early visual areas such as V1 are also activated by texture detection and surface segregation processes (Scholte et al., 2008).

In conclusion, we find evidence for variations in the properties of retinotopic maps for different motion-based stimuli. In particular, we find clear retinotopic maps for the a stimulus defined by a moving bar of dots against a blank background, but much weaker maps when the bar was defined by coherently moving dots against a background of incoherent dots, or by transparent compared to non-transparent motion. However, rather than this reflecting a change in responsivity of neurons in different visual areas to different motion properties, we suggest that the general visibility or salience of a stimulus is the most important driver of pRF properties, in particular in the higher dorsal visual areas, as stimuli defined by size differences produced very similar maps to a global motion stimulus.

**Supplementary Materials:** Video S1: Example bar-only stimulus, Video S2: Example kinetic stimulus, Video S3: Example global stimulus, Video S4: Example transparent bar-only stimulus, Video S5: Example transparent motion stimulus, Video S6: Example size-defined stimulus

**Acknowledgments:** Supported by ERC Starting Grant WMOSPOTWU to DSS, and Career Development Award MR/K024817/1 from the UK Medical Research Council to JAG.

**Author Contributions:** All authors conceived and designed the experiments and performed the experiments; A.H. and D.S.S. analysed the data; D.S.S. contributed analysis tools; A.H. wrote the paper; all authors edited the paper and approved the final version.

**Conflicts of Interest:** The authors declare no conflict of interest. The funding sponsors had no role in the design of the study; in the collection, analyses, or interpretation of data; in the writing of the manuscript, and in the decision to publish the results.

## References

- Adelson, E.H., Movshon, J.A., 1982. Phenomenal coherence of moving visual patterns. *Nature* 300, 523–525.
- Allen, H.A., Ledge, T., 2003. Attentional modulation of threshold sensitivity to first-order motion and second-order motion patterns. *Vision Res.* 43, 2927–2936. <https://doi.org/10.1016/j.visres.2003.07.005>
- Alvarez, I., Haas, D., A, B., Clark, C.A., Rees, G., Schwarzkopf, D.S., 2015. Comparing different stimulus configurations for population receptive field mapping in human fMRI. *Front. Hum. Neurosci.* 9. <https://doi.org/10.3389/fnhum.2015.00096>
- Amano, K., Wandell, B.A., Dumoulin, S.O., 2009. Visual field maps, population receptive field sizes, and visual field coverage in the human MT+ complex. *J. Neurophysiol.* 102, 2704–2718. <https://doi.org/10.1152/jn.00102.2009>
- Anzai, A., DeAngelis, G.C., 2010. Neural computations underlying depth perception. *Curr. Opin. Neurobiol.* 20, 367–375. <https://doi.org/10.1016/j.conb.2010.04.006>
- Backus, B.T., Fleet, D.J., Parker, A.J., Heeger, D.J., 2001. Human cortical activity correlates with stereoscopic depth perception. *J. Neurophysiol.* 86, 2054–2068. <https://doi.org/10.1152/jn.2001.86.4.2054>
- Ban, H., Preston, T.J., Meeson, A., Welchman, A.E., 2012. The integration of motion and disparity cues to depth in dorsal visual cortex. *Nat. Neurosci.* 15, 636–643. <https://doi.org/10.1038/nn.3046>
- Bates, D., Mächler, M., Bolker, B., Walker, S., 2014. Fitting Linear Mixed-Effects Models using lme4. *ArXiv14065823 Stat.*
- Braddick, O.J., O'Brien, J.M., Wattam-Bell, J., Atkinson, J., Hartley, T., Turner, R., 2001. Brain areas sensitive to coherent visual motion. *Perception* 30, 61–72. <https://doi.org/10.1068/p3048>
- Brainard, D.H., 1997. The Psychophysics Toolbox. *Spat. Vis.* 10, 433–436.
- Breuer, F.A., Blaimer, M., Heidemann, R.M., Mueller, M.F., Griswold, M.A., Jakob, P.M., 2005. Controlled aliasing in parallel imaging results in higher acceleration (CAIPIRINHA) for multi-slice imaging. *Magn. Reson. Med.* 53, 684–691. <https://doi.org/10.1002/mrm.20401>
- Britten, K.H., Shadlen, M.N., Newsome, W.T., Movshon, J.A., 1993. Responses of neurons in macaque MT to stochastic motion signals. *Vis. Neurosci.* 10, 1157–1169.
- Britten, K.H., Shadlen, M.N., Newsome, W.T., Movshon, J.A., 1992. The analysis of visual motion: a comparison of neuronal and psychophysical performance. *J. Neurosci. Off. J. Soc. Neurosci.* 12, 4745–4765.
- Chen, S.C., Morley, J.W., Solomon, S.G., 2015. Spatial precision of population activity in primate area MT. *J. Neurophysiol.* jn.00152.2015. <https://doi.org/10.1152/jn.00152.2015>
- Dale, A.M., Fischl, B., Sereno, M.I., 1999. Cortical surface-based analysis. I. Segmentation and surface reconstruction. *NeuroImage* 9, 179–194. <https://doi.org/10.1006/nimg.1998.0395>
- De Bruyn, B., 1997. Blending Transparent Motion Patterns in Peripheral Vision. *Vision Res.* 37, 645–648. [https://doi.org/10.1016/S0042-6989\(96\)00117-4](https://doi.org/10.1016/S0042-6989(96)00117-4)

- Dumoulin, S.O., Hess, R.F., May, K.A., Harvey, B.M., Rokers, B., Barendregt, M., 2014. Contour extracting networks in early extrastriate cortex. *J. Vis.* 14, 18–18. <https://doi.org/10.1167/14.5.18>
- Dumoulin, S.O., Wandell, B.A., 2008. Population receptive field estimates in human visual cortex. *NeuroImage* 39, 647–660. <https://doi.org/10.1016/j.neuroimage.2007.09.034>
- Dupont, P., Orban, G.A., De Bruyn, B., Verbruggen, A., Mortelmans, L., 1994. Many areas in the human brain respond to visual motion. *J. Neurophysiol.* 72, 1420–1424. <https://doi.org/10.1152/jn.1994.72.3.1420>
- Edwards, M., Cassanello, C.R., Kalia, K., 2012. Adaptation state of the local-motion-pooling units determines the nature of the motion aftereffect to transparent motion. *Vision Res.* 64, 23–25. <https://doi.org/10.1016/j.visres.2012.05.006>
- Edwards, M., Greenwood, J.A., 2005. The perception of motion transparency: a signal-to-noise limit. *Vision Res.* 45, 1877–1884. <https://doi.org/10.1016/j.visres.2005.01.026>
- Edwards, M., Nishida, S., 1999. Global-motion detection with transparent-motion signals. *Vision Res.* 39, 2239–2249.
- Felleman, D.J., Van Essen, D.C., 1991. Distributed hierarchical processing in the primate cerebral cortex. *Cereb. Cortex N. Y. N* 1991 1, 1–47.
- Fischl, B., Sereno, M.I., Dale, A.M., 1999. Cortical surface-based analysis. II: Inflation, flattening, and a surface-based coordinate system. *NeuroImage* 9, 195–207. <https://doi.org/10.1006/nimg.1998.0396>
- Haas, B. de, Schwarzkopf, D.S., 2018. Spatially selective responses to Kanizsa and occlusion stimuli in human visual cortex. *Sci. Rep.* 8, 611. <https://doi.org/10.1038/s41598-017-19121-z>
- Haas, B. de, Schwarzkopf, D.S., Anderson, E.J., Rees, G., 2014. Perceptual load affects spatial tuning of neuronal populations in human early visual cortex. *Curr. Biol.* 24, R66–R67. <https://doi.org/10.1016/j.cub.2013.11.061>
- Harvey, B.M., Dumoulin, S.O., 2011. The Relationship between Cortical Magnification Factor and Population Receptive Field Size in Human Visual Cortex: Constancies in Cortical Architecture. *J. Neurosci.* 31, 13604–13612. <https://doi.org/10.1523/JNEUROSCI.2572-11.2011>
- Heeger, D.J., Simoncelli, E.P., Movshon, J.A., 1996. Computational models of cortical visual processing. *Proc. Natl. Acad. Sci.* 93, 623–627.
- Hess, R.F., Aen-Stockdale, C., 2008. Global motion processing: The effect of spatial scale and eccentricity. *J. Vis.* 8, 11.1–11. <https://doi.org/10.1167/8.4.11>
- Huk, A.C., Ress, D., Heeger, D.J., 2001. Neuronal basis of the motion aftereffect reconsidered. *Neuron* 32, 161–172.
- Kanai, R., Paffen, C.L.E., Gerbino, W., Verstraten, F.A.J., 2004. Blindness to inconsistent local signals in motion transparency from oscillating dots. *Vision Res.* 44, 2207–2212. <https://doi.org/10.1016/j.visres.2004.04.010>
- Kastner, S., DeSimone, K., Konen, C.S., Szczepanski, S.M., Weiner, K.S., Schneider, K.A., 2007. Topographic maps in human frontal cortex revealed in memory-guided saccade and spatial working-memory tasks. *J. Neurophysiol.* 97, 3494–3507. <https://doi.org/10.1152/jn.00010.2007>
- Kay, K.N., Weiner, K.S., Grill-Spector, K., 2015. Attention Reduces Spatial Uncertainty in Human Ventral Temporal Cortex. *Curr. Biol.* 25, 595–600. <https://doi.org/10.1016/j.cub.2014.12.050>



- Klein, B.P., Harvey, B.M., Dumoulin, S.O., 2014. Attraction of position preference by spatial attention throughout human visual cortex. *Neuron* 84, 227–237. <https://doi.org/10.1016/j.neuron.2014.08.047>
- Knapen, T., Es, D. van, Barendregt, M., 2018. Mapping the Dark Side: Visual Selectivity of Default Network Deactivations. *bioRxiv* 292524. <https://doi.org/10.1101/292524>
- Lagarias, J., Reeds, J., Wright, M., Wright, P., 1998. Convergence Properties of the Nelder--Mead Simplex Method in Low Dimensions. *SIAM J. Optim.* 9, 112–147. <https://doi.org/10.1137/S1052623496303470>
- Larsson, J., Heeger, D.J., 2006. Two retinotopic visual areas in human lateral occipital cortex. *J. Neurosci. Off. J. Soc. Neurosci.* 26, 13128–13142. <https://doi.org/10.1523/JNEUROSCI.1657-06.2006>
- Leventhal, A.G., Wang, Y., Schmolesky, M.T., Zhou, Y., 1998. Neural correlates of boundary perception. *Vis. Neurosci.* 15, 1107–1118.
- Lu, Z.L., Liu, C.Q., Doshier, B.A., 2000. Attention mechanisms for multi-location first- and second-order motion perception. *Vision Res.* 40, 173–186.
- Marcar, V.L., Raiguel, S.E., Xiao, D., Orban, G.A., 2000. Processing of kinetically defined boundaries in areas V1 and V2 of the macaque monkey. *J. Neurophysiol.* 84, 2786–2798. <https://doi.org/10.1152/jn.2000.84.6.2786>
- Marr, D., Ullman, S., 1981. Directional selectivity and its use in early visual processing. *Proc. R. Soc. Lond. Ser. B Contain. Pap. Biol. Character R. Soc. G. B.* 211, 151–180.
- McKeefry, D.J., Watson, J.D., Frackowiak, R.S., Fong, K., Zeki, S., 1997. The activity in human areas V1/V2, V3, and V5 during the perception of coherent and incoherent motion. *NeuroImage* 5, 1–12. <https://doi.org/10.1006/nimg.1996.0246>
- Moutsiana, C., de Haas, B., Papageorgiou, A., van Dijk, J.A., Balraj, A., Greenwood, J.A., Schwarzkopf, D.S., 2016. Cortical idiosyncrasies predict the perception of object size. *Nat. Commun.* 7, 12110. <https://doi.org/10.1038/ncomms12110>
- Muckli, L., Singer, W., Zanella, F.E., Goebel, R., 2002. Integration of Multiple Motion Vectors Over Space: An fMRI Study of Transparent Motion Perception. *NeuroImage* 16, 843–856. <https://doi.org/10.1006/nimg.2002.1085>
- Murray, S.O., Boyaci, H., Kersten, D., 2006. The representation of perceived angular size in human primary visual cortex. *Nat. Neurosci.* 9, 429–434. <https://doi.org/10.1038/nn1641>
- Nakayama, K., 1985. Biological image motion processing: A review. *Vision Res.* 25, 625–660. [https://doi.org/10.1016/0042-6989\(85\)90171-3](https://doi.org/10.1016/0042-6989(85)90171-3)
- Nelder, J.A., Mead, R., 1965. A Simplex Method for Function Minimization. *Comput. J.* 7, 308–313. <https://doi.org/10.1093/comjnl/7.4.308>
- Newsome, W.T., Paré, E.B., 1988. A selective impairment of motion perception following lesions of the middle temporal visual area (MT). *J. Neurosci. Off. J. Soc. Neurosci.* 8, 2201–2211.
- Nishida, S., 2011. Advancement of motion psychophysics: Review 2001–2010. *J. Vis.* 11. <https://doi.org/10.1167/11.5.11>
- Pelli, D.G., 1997. The VideoToolbox software for visual psychophysics: transforming numbers into movies. *Spat. Vis.* 10, 437–442.
- Pitzalis, S., Sereno, M.I., Committeri, G., Fattori, P., Galati, G., Patria, F., Galletti, C., 2010. Human V6: The Medial Motion Area. *Cereb. Cortex N. Y. NY* 20, 411–424. <https://doi.org/10.1093/cercor/bhp112>

- Pooresmaeili, A., Arrighi, R., Biagi, L., Morrone, M.C., 2013. Blood Oxygen Level-Dependent Activation of the Primary Visual Cortex Predicts Size Adaptation Illusion. *J. Neurosci.* 33, 15999–16008. <https://doi.org/10.1523/JNEUROSCI.1770-13.2013>
- Qian, N., Andersen, R.A., 1994. Transparent motion perception as detection of unbalanced motion signals. II. Physiology. *J. Neurosci. Off. J. Soc. Neurosci.* 14, 7367–7380.
- Qian, N., Andersen, R.A., Adelson, E.H., 1994. Transparent motion perception as detection of unbalanced motion signals. I. Psychophysics. *J. Neurosci. Off. J. Soc. Neurosci.* 14, 7357–7366.
- Raymond, J.E., 1994. Directional anisotropy of motion sensitivity across the visual field. *Vision Res.* 34, 1029–1037.
- Regan, D., Beverley, K.I., 1984. Figure–ground segregation by motion contrast and by luminance contrast. *JOSA A* 1, 433–442. <https://doi.org/10.1364/JOSAA.1.000433>
- Regan, D., Hamstra, S., 1991. Shape discrimination for motion-defined and contrast-defined form: squareness in special. *Perception* 20, 315–336. <https://doi.org/10.1068/p200315>
- Russell, L., 2018. emmeans: Estimated Marginal Means, aka Least-Squares Means. R package version 1.2.1.
- Saygin, A.P., Sereno, M.I., 2008. Retinotopy and attention in human occipital, temporal, parietal, and frontal cortex. *Cereb. Cortex N. Y. N* 1991 18, 2158–2168. <https://doi.org/10.1093/cercor/bhm242>
- Scase, M.O., Braddick, O.J., Raymond, J.E., 1996. What is Noise for the Motion System? *Vision Res.* 36, 2579–2586. [https://doi.org/10.1016/0042-6989\(95\)00325-8](https://doi.org/10.1016/0042-6989(95)00325-8)
- Scholte, H.S., Jolij, J., Fahrenfort, J.J., Lamme, V.A.F., 2008. Feedforward and recurrent processing in scene segmentation: electroencephalography and functional magnetic resonance imaging. *J. Cogn. Neurosci.* 20, 2097–2109. <https://doi.org/10.1162/jocn.2008.20142>
- Schwarzkopf, D.S., Anderson, E.J., Haas, B. de, White, S.J., Rees, G., 2014. Larger Extrastriate Population Receptive Fields in Autism Spectrum Disorders. *J. Neurosci.* 34, 2713–2724. <https://doi.org/10.1523/JNEUROSCI.4416-13.2014>
- Sereno, M.I., Dale, A.M., Reppas, J.B., Kwong, K.K., Belliveau, J.W., Brady, T.J., Rosen, B.R., Tootell, R.B., 1995. Borders of multiple visual areas in humans revealed by functional magnetic resonance imaging. *Science* 268, 889–893.
- Simoncelli, E.P., Heeger, D.J., 1998. A model of neuronal responses in visual area MT. *Vision Res.* 38, 743–761. [https://doi.org/10.1016/S0042-6989\(97\)00183-1](https://doi.org/10.1016/S0042-6989(97)00183-1)
- Snowden, R.J., Treue, S., Erickson, R.G., Andersen, R.A., 1991. The response of area MT and V1 neurons to transparent motion. *J. Neurosci.* 11, 2768–2785. <https://doi.org/10.1523/JNEUROSCI.11-09-02768.1991>
- Snowden, R.J., Verstraten, F.A.J., 1999. Motion transparency: making models of motion perception transparent. *Trends Cogn. Sci.* 3, 369–377. [https://doi.org/10.1016/S1364-6613\(99\)01381-9](https://doi.org/10.1016/S1364-6613(99)01381-9)
- Sperandio, I., Chouinard, P.A., Goodale, M.A., 2012. Retinotopic activity in V1 reflects the perceived and not the retinal size of an afterimage. *Nat. Neurosci.* 15, 540–542. <https://doi.org/10.1038/nn.3069>
- Sunaert, S., Van Hecke, P., Marchal, G., Orban, G.A., 1999. Motion-responsive regions of the human brain. *Exp. Brain Res.* 127, 355–370.

- Tootell, R.B.H., Hadjikhani, N., Hall, E.K., Marrett, S., Vanduffel, W., Vaughan, J.T., Dale, A.M., 1998. The Retinotopy of Visual Spatial Attention. *Neuron* 21, 1409–1422. [https://doi.org/10.1016/S0896-6273\(00\)80659-5](https://doi.org/10.1016/S0896-6273(00)80659-5)
- Tootell, R.B.H., Mendola, J.D., Hadjikhani, N.K., Ledden, P.J., Liu, A.K., Reppas, J.B., Sereno, M.I., Dale, A.M., 1997. Functional Analysis of V3A and Related Areas in Human Visual Cortex. *J. Neurosci.* 17, 7060–7078.
- Tsao, D.Y., Vanduffel, W., Sasaki, Y., Fize, D., Knutsen, T.A., Mandeville, J.B., Wald, L.L., Dale, A.M., Rosen, B.R., Essen, D.C.V., Livingstone, M.S., Orban, G.A., Tootell, R.B.H., 2003. Stereopsis Activates V3A and Caudal Intraparietal Areas in Macaques and Humans. *Neuron* 39, 555–568. [https://doi.org/10.1016/S0896-6273\(03\)00459-8](https://doi.org/10.1016/S0896-6273(03)00459-8)
- Tyler, C.W., Likova, L.T., Kontsevich, L.L., Wade, A.R., 2006. The specificity of cortical region KO to depth structure. *NeuroImage* 30, 228–238. <https://doi.org/10.1016/j.neuroimage.2005.09.067>
- van Dijk, J.A., de Haas, B., Moutsiana, C., Schwarzkopf, D.S., 2016. Intersession reliability of population receptive field estimates. *NeuroImage* 143, 293–303. <https://doi.org/10.1016/j.neuroimage.2016.09.013>
- Van Essen, D.C., Gallant, J.L., 1994. Neural mechanisms of form and motion processing in the primate visual system. *Neuron* 13, 1–10.
- Van Oostende, S., Sunaert, S., Van Hecke, P., Marchal, G., Orban, G.A., 1997. The kinetic occipital (KO) region in man: an fMRI study. *Cereb. Cortex N. Y. N* 1991 7, 690–701.
- Vidnyánszky, Z., Blaser, E., Papathomas, T.V., 2002. Motion integration during motion aftereffects. *Trends Cogn. Sci.* 6, 157–161. [https://doi.org/10.1016/S1364-6613\(02\)01871-5](https://doi.org/10.1016/S1364-6613(02)01871-5)
- Vo, V.A., Sprague, T.C., Serences, J.T., 2017. Spatial Tuning Shifts Increase the Discriminability and Fidelity of Population Codes in Visual Cortex. *J. Neurosci. Off. J. Soc. Neurosci.* 37, 3386–3401. <https://doi.org/10.1523/JNEUROSCI.3484-16.2017>
- Wallach, H., 1935. Über visuell wahrgenommene Bewegungsrichtung. *Psychol. Forsch.* 20, 325–380. <https://doi.org/10.1007/BF02409790>
- Watamaniuk, S.N., 1993. Ideal observer for discrimination of the global direction of dynamic random-dot stimuli. *J. Opt. Soc. Am. A* 10, 16–28.
- Williams, D.W., Sekuler, R., 1984. Coherent global motion percepts from stochastic local motions. *Vision Res.* 24, 55–62. [https://doi.org/10.1016/0042-6989\(84\)90144-5](https://doi.org/10.1016/0042-6989(84)90144-5)
- Yildirim, F., Carvalho, J., Cornelissen, F.W., 2018. A second-order orientation-contrast stimulus for population-receptive-field-based retinotopic mapping. *NeuroImage, Pushing the spatio-temporal limits of MRI and fMRI* 164, 183–193. <https://doi.org/10.1016/j.neuroimage.2017.06.073>
- Zeki, S., Perry, R.J., Bartels, A., 2003. The Processing of Kinetic Contours in the Brain. *Cereb. Cortex* 13, 189–202. <https://doi.org/10.1093/cercor/13.2.189>